Surface reactivity of $V_2O_5(001)$: Effects of vacancies, protonation, hydroxylation, and chlorination

Ana Suarez Negreira,[1] Shela Aboud,[2] and Jennifer Wilcox[2,*]

[1]*Department of Chemical Engineering, Stanford University, Stanford, California 94305-2220, USA*

[2]*Department of Energy Resources Engineering, Stanford University, Stanford, California 94305-2220, USA*

(Received 21 August 2010; revised manuscript received 22 November 2010; published 28 January 2011)

Using density-functional theory we analyze the thermodynamic stability of partially reduced, protonated, hydroxylated, and chlorinated $V_2O_5(001)$ surfaces under flue gas conditions. These surfaces are characterized geometrically through surface relaxation calculations and electronically through charge distribution and density-of-states analysis to understand the change in surface reactivity under different pressure and temperature conditions, with a primary focus on coal-fired flue gas conditions. The stoichiometric surface is found to be the most favorable termination under flue gas conditions, but at low oxygen partial pressures (i.e., ultra-high-vacuum conditions) and elevated temperatures, the partially reduced $V_2O_5(001)$ surfaces with one or two vanadyl oxygen vacancies are found to be stable. A surface semiconductor-to-metal transformation takes place with the addition of oxygen vacancies indicated by a decrease in the band gap. The protonation of the $V_2O_5(001)$ surface only takes place at low oxygen partial pressures where the main source or sink of hydrogen atoms comes from H_2. The study of the thermodynamic stability of protonated surfaces and surfaces with dissociated water with both H– and OH– groups indicated that these surfaces are not stable under flue gas conditions. Chlorinated surfaces were not stable under the flue gas and the coverage conditions tested. Larger HCl concentrations or smaller coverages may lead to stable chlorinated structures; however, the small coverages required to accurately represent the chlorine flue gas concentrations would require much larger unit-cell sizes that would be too computationally expensive. From this work it is evident that the stoichiometric surface of V_2O_5 is the most stable under flue gas conditions, and likely reactivity corresponding to NO_x reduction, surface chlorination, and mercury oxidation stems from support effects on the vanadia catalyst, which influences the vanadium oxidation state and subsequent surface reactivity.

DOI: 10.1103/PhysRevB.83.045423 PACS number(s): 82.65.+r, 82.20.Wt, 68.43.−h

I. INTRODUCTION

For the past 30 years, Japan, Europe, and the United States have been using selective catalytic reduction (SCR) units to control NO_x emissions from natural gas or coal-fired power plants.[1] During NO_x reduction, NO is reduced by ammonia (NH_3), which is injected at high temperatures (>600 K) upstream.[2] An undesired secondary reaction during NO_x reduction is the oxidation of sulfur dioxide to sulfur trioxide (SO_3) over the catalyst when it reacts with NH_3 and water, producing ammonium bisulfate or ammonium sulfate, which may subsequently damage the SCR reactor.[3] Vanadium pentoxide (V_2O_5) has been used extensively as a catalyst material in SCR units because of its high catalytic activity, high thermal stability, and SO_3 poisoning resistance.[3] A co-benefit of the V_2O_5-based SCR catalyst is the enhancement of mercury oxidation, in which elemental mercury (Hg^0) is converted to its oxidized form (Hg^{2+}).[4] Oxidized mercury is highly soluble in aqueous solutions, making its removal by conventional wet flue gas desulfurization units possible. Atmospheric levels of gaseous mercury have raised public concern due to long-term irreversible effects on the environment and human health.[1] Several studies have indicated that mercury oxidation performs even better at lower temperatures (≈400 K) downstream of the SRC system;[2] therefore, temperature seems to play an important role in the V_2O_5 catalyst reactivity.

Although numerous experimental studies indicate that V_2O_5 catalyzes mercury oxidation, the detailed mechanism across the SCR catalyst is still unknown. Studies carried out by Senior and Linjewile[5] suggest that the reaction follows an Eley-Rideal mechanism in which Hg adsorbs to the surface of V_2O_5 and is later oxidized by HCl present in the gas phase. However, Niksa and Fujiwara[6] suggest that the oxidation of Hg^0 to Hg^{2+} actually takes place through a Langmuir-Hinshelwood mechanism where gas-phase Hg^0 reacts with HCl that has previously been adsorbed onto the V_2O_5 catalyst. Experimental work in characterizing Hg adsorption and oxidation across the V_2O_5 in a bench-scale SCR system was carried out by Eom *et al.*[7] and He *et al.*[8] and confirmed negligible Hg oxidation activity on the SCR catalyst when HCl is absent. By injecting HCl over a V_2O_5 surface saturated with Hg and observing how the surface released Hg in favor of HCl adsorption, He *et al.* were able to conclude that HCl has a higher affinity for the active sites in the V_2O_5 catalyst over Hg. Results from Eom *et al.*[7] suggest that Hg and HCl actually compete for the same V_2O_5 adsorption sites which support the Langmuir-Hinshelwood mechanism. Those experimental studies were performed under constant temperature (300 °C in He *et al.*[8] and 350 °C in Eom *et al.*[7]) so the effect of the temperature on the mechanism as well as the kinetics that govern the interaction of HCl and Hg with the surface of V_2O_5 have not yet been investigated. The current work aims to determine the extent of reactivity of the $V_2O_5(001)$ surface under flue gas conditions in order to provide a foundation for further elucidating the role of chlorine in Hg^0 oxidation across this catalyst. The experimental characterization of the (001) surface by scanning tunneling microscopy (STM)[9–12] and atomic force microscopy (AFM),[12,13] suggest that this surface is the most energetically favorable, prompting the use of this surface in this study. A cross-section and top view of the $V_2O_5(001)$ surface is shown in Fig. 1.

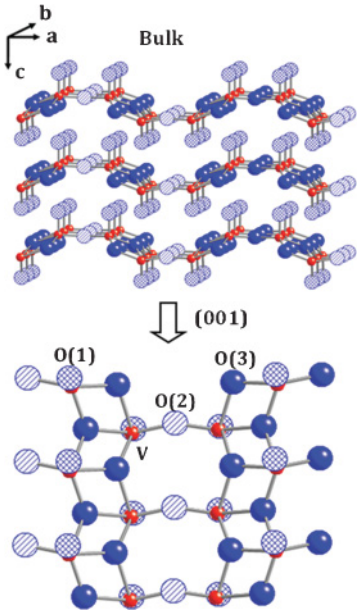

FIG. 1. (Color online) View of the two-layer V_2O_5 slab (top) and top view of the V_2O_5(001) surface (bottom). V atoms are the red small solid spheres while the different O atoms are the big blue spheres [solid, O(3); hatched, O(2); cross-hatched, O(1)].

In addition to HCl and temperature, the catalytic properties of the V_2O_5 surface will be influenced by post-combustion gas species such as O_2 and H_2O and acid species such as SO_x and NO_x. Ganduglia-Pivorano and Sauer[14] studied the stability of partially reduced V_2O_5(001) surfaces at finite temperatures as a function of the oxygen partial pressure in the gas phase. They found that at standard pressure and moderate temperatures (≈800 K) V_2O_5 is the most thermodynamically stable oxide and that oxygen vacancies only occur under extreme reducing conditions ($p_O = 10^{-13}$ atm). Goclon *et al.*[15] indicated that the energy required for oxygen vacancy formation on low-index V_2O_5 surfaces can be decreased by the adsorption of atomic hydrogen, followed by the desorption of the hydroxyl group. Their study for the (001) surface [indexed as (010) in their paper] suggests that the process of adsorption of hydrogen atoms yields a slight elongation of the V–O bond, making it easier to break, leaving behind an oxygen vacancy. They suggest that the protonation of the vanadyl oxygen [O(1) as shown in Fig. 1] and the formation of this oxygen vacancy is the most energetically favorable process on the (001) surface. Although, the experimental work of Tepper *et al.*[16] supports the idea that dosing atomic hydrogen on the V_2O_5(001) surface leads to the reduction of this surface, they suggested that the most favorable process may be the protonation of the O(2) oxygen atom, followed by the desorption of this hydroxyl group, in contrast with the results by Glocon *et al.*

Desorption of the hydroxyl groups from the surface could be driven by the formation and thermal desorption of water molecules, as suggested by the experimental work of Busca *et al.*[17] which concluded that water desorbs from the V_2O_5 substrate at 383 K. Sturm *et al.*[18] reported binding energies of 0.64 and 0.44 eV for molecular and dissociated water on vanadyl oxygen defected V_2O_5(001) surface supported on a Au(111) film layer. In the same surface, Göbke *et al.*[19] suggests that adsorption/dissociation of methanol leading to adsorbed methoxy and hydroxy groups only takes place on the presence of vanadyl defects since the stoichiometric surface (terminated with vanadyl groups) is unreactive for this reaction. Since vanadyl oxygen vacancies play an important role in the reactivity of V_2O_5(001) surface for those reactions, it is important to study their stability under flue gas conditions to see their influence in Hg oxidation. While much of the previous experimental work has been carried out on supported V_2O_5, the scope of this work is to investigate the reactivity of unsupported V_2O_5 in the presence of flue gas species, H_2O, HCl, O_2, and H_2, as a reference calculation for future studies on supported V_2O_5 catalyst. Using density functional theory (DFT) to simulate the supported V_2O_5 will be considered in future work, but it will be considered in future work.

The goal of the current work is to investigate the surface structure and reactivity of V_2O_5(001) under flue gas conditions (flue gas composition, temperature, and pressure) using DFT calculations. This study will be used as a first step in elucidating the mechanism that governs the heterogeneous Hg oxidation pathway across V_2O_5. Although numerous studies have been carried out to analyze the reactivity of the V_2O_5(001) surface based on the analysis of adsorption energies,[15,20–24] little work has been carried out on the analysis of the thermodynamic stability of these surfaces. The thermodynamic stability of the partially reduced V_2O_5(001) surface and possible protonated/hydroxylated V_2O_5(001) surfaces are analyzed as a function of oxygen partial pressure at finite temperatures by carrying out *ab initio* thermodynamic calculations. The interactions between HCl and the surface will be analyzed by studying the stability of chlorinated V_2O_5(001) surfaces as a function of the temperature and partial pressure of HCl. Gas-surface interactions depend not only on the local chemical/electronic environment but on the capacity of the surface to relax; therefore, it is important to investigate the change in bond distances along with electronic density of states (DOS) of the surface with the formation of oxygen vacancies, surface protonation, and surface chlorination to fully understand the change in surface reactivity.

II. COMPUTATIONAL METHODOLOGY

A. Density functional theory

Plane-wave DFT calculations were performed using the Vienna Ab Initio Simulation Package (VASP),[25] using the Perdew-Burke-Enzerhoff (PBE)[26] generalized-gradient approximation (GGA). A projector augmented wave (PAW),[27] pseudopotential is used with an optimized energy cutoff of 600 eV. A $7 \times 7 \times 7$ grid was used for the V_2O_5 bulk calculations, with a convergence criterion of 10^{-4} eV. The V_2O_5(001) surface was simulated with a $1 \times 1 \times 2$-unit-cell double-surface slab, with the slab thickness benchmarked to ensure bulklike behavior of the central atoms. The slabs were separated by a vacuum layer of 30 Å to prevent interaction between periodic images, and symmetric double-vacuum slabs were used to cancel any dipole moment potentially created from periodic images. In any of the surface-gas phase interactions, symmetric slabs were used to cancel any dipole moment that could be created due to the periodic

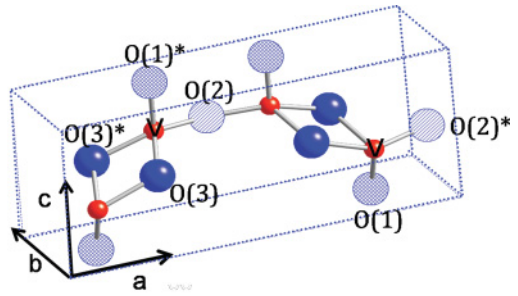

FIG. 2. (Color online) V_2O_5 unit cell.

conditions. For the surface simulations the number of k points for the Brillion zone integration was chosen according to the Monkhorst-Pack[28] scheme to be $3 \times 3 \times 1$. The positions of all atoms were relaxed using a conjugate-gradient algorithm. The DFT parameters are calibrated by characterizing the geometric, electronic and magnetic properties of bulk V_2O_5. Bulk V_2O_5 follows by an orthorhombic lattice layer-type structure. The three crystallographic axes that comprise the unit cell are shown in Fig. 2.

The V_2O_5 unit cell used in this work consists of 14 atoms, that is, 4 vanadium and 10 oxygen atoms. There are three types of oxygen atoms, differing by their coordination number with the vanadium atoms. The vanadyl oxygen, O(1), is double bonded with the vanadium atom perpendicular to the (001) plane. An O(2) atom bridges two vanadium atoms in the a direction. The three coordinated oxygen atoms, O(3), are extended in the a and b directions. V_2O_5 is a layerlike material with a no-covalent interaction between the layers, making it easy for cleavage along the (001) plane.[29]

The optimization of the V_2O_5 unit cell was carried out fixing two of the unit vectors and then varying the third unit vector until the minimum energy value for the structure was obtained. The optimal unit vectors predictions presented in Table I are compared against x-ray diffraction measurements and other DFT predictions available in the literature. This table shows reasonable agreement for a and b unit vectors. Unlike a and b, there is a larger range of values for the unit vector c, due to the fact that DFT does a poor job of properly accounting for the existing van der Waals-based interlayer interaction.

To study the accuracy of the simulated electronic structure, DOS calculations are carried out and the band gap of V_2O_5 is compared against experiment. The DOS is obtained by projecting the electronic wave functions onto spherical harmonics centered at each of the vanadium and oxygen atoms.

TABLE I. Predicted and experimental unit vector parameters.

Source	a (Å)	b (Å)	c (Å)
This work	11.53	3.58	4.76
Experiment[a]	11.51	3.56	4.37
Goclon *et al.*[b]	11.65	3.57	4.66
Kresse *et al.*[c]	11.65	3.57	4.69
GP *et al.*[d]	11.62	3.59	4.44

[a]Reference 30.
[b]Reference 31.
[c]Reference 32.
[d]Reference 14.

The calculated value of the indirect band gap of V_2O_5 is found to be 1.78 eV, which is in excellent agreement with the experimentally measured value of 1.8 eV measured using STM.[33] Although DFT calculations tend to underestimate the band gap, the agreement between our predicted and the experimental values suggest that our PBE functional can properly characterize the electronic properties of this surface. This is an important assessment of the validity of this approach for calculating the thermodynamic stability of this surface under flue gas conditions. Spin-polarized calculations were also carried out and it was found that the inclusion of spin polarization did not influence the stoichiometric surface. The influence of the spin polarization on the energy values for the case of partially reduced surfaces was small [0% for single O(1) vacancies and 2% for double O(1) vacancies] and similar effects were observed for some protonated surfaces (0.03%). Due to the small influence in the energy values, further calculations for the protonated/hydroxilated and chlorinated surfaces were carried out without including spin effects although other DFT investigations[14,29] have included spin.

Although plane-wave DFT total energy calculations for the gas-phase molecules (H_2O, O_2, Cl_2, and HCl) are less accurate than for extended systems such as bulk materials or surfaces,[34,35] to maintain consistency of the results, calculated values of chemical potentials for the gas species have been used. A detailed explanation will be provided in the next section regarding the relationship between these chemical potential values and the total energies of isolated molecules calculated with DFT in a $20 \times 20 \times 20$ Å^3 periodic box. As Mason *et al.*[34] discussed in their work, special attention should be paid to the inherent error associated with O_2 due to its triplet ground state and short bond distance. For the case of O_2, it was necessary to carry out spin-polarized calculations to compute accurate total and atomization energies per O_2 molecule.

B. *Ab initio* thermodynamics calculations

Tuning the morphology and the reactivity of a given surface material by modifying the gas-phase composition and temperature is possible and *ab initio* thermodynamic calculations can provide the insight into the surface chemistry as a function of these conditions. This approach is used to predict the relative thermodynamic stability and composition of different terminated V_2O_5(001) surfaces in contact with a flue gas environment as a function of temperature (T) and pressure (p). Relevant temperatures for a coal-fired power plant are 60 °C, 135 °C, and 175 °C (333 K, 410 K, and 449 K, respectively)[36] so a wide range of temperatures is investigated (100 K–1000 K), paying special attention to the reactivity at 500 K and 1000 K, which are used as bracketing temperature references for the SCR catalyst conditions. The compositions of a typical flue gas for burning bituminous coal (e.g., Appalachian medium sulfur) and lignite coal (e.g., Wyodak) were calculated using the Integrated Environmental Control Model (IECM),[37] a power-plant simulation model developed by Rubin *et al.* at Carnegie Mellon University, with the conditions shown in Table II. Since we are interested in studying the change of the surface upon interaction with HCl, the lignite coal-fired flue gas composition was chosen due to its higher HCl content.

TABLE II. Typical constituents and mass fractions of flue gas (Ref. 37).

Components	Concentration	Components	Concentration
Nitrogen (N_2)	66.13 wt%	Sulfur dioxide (SO_2)	0.05 wt
Oxygen (O_2)	4.61 wt%	Sulfur acid (equivalent SO_3)	1.4 ppm
Water vapor (H_2O)	9.75 wt%	Nitric oxide (NO)	82.7 ppm
Hydrogen (H_2)	Negligible	Nitric dioxide (NO_2)	6.7 ppm
Carbon dioxide (CO_2)	18.30 wt%	Ammonia (NH_3)	1 ppm
Hydrochloric acid (HCl)	4.1 ppm	Argon (Ar)	1.12 wt%

The surface free energy, γ, of a semi-infinite slab with two equivalent surfaces in contact with a gas-phase reservoir at a given temperature T and pressure p is given by[35]

$$\gamma\left(T,\{p_i\}\right)=\frac{1}{2A}\left[G\left(T,\{p_i\},N_i\right)-\sum_i N_i\mu_i\left(T,p_i\right)\right], \quad (1)$$

where $G(T,p_i,N_i)$ is the Gibbs free energy of the system, N_i the number of system species, and μ_i the chemical potential of those species, which for protonated/hydroxylated and chlorinated V_2O_5 surfaces are μ_V, μ_O, μ_{Cl}, and μ_H, respectively. Assuming that there is adequate bulk material to act as a reservoir, the chemical potentials of the constituent elements are related by the Gibbs free energy per formula unit, g_i, of the species present in the system. The relation between the Gibbs free energy and the DFT-calculated free energies in Eq. (1) has been explained in detail in previous DFT studies,[33,38–40] where they showed that the Gibbs free energy can be approximated by the Helmholtz free energy when working with pressures below 100 atm. Some studies[35,40] suggested that at 0 K the contribution to the zero-point vibrations are negligible, which makes it possible to equate the Helmholtz free energy to the total electronic energy, E_i, calculated with DFT. In this study we consider that the only contribution to the vibrational free energy is from the hydrogen atoms of the bound water and hydroxyl groups, which can be calculated within the harmonic oscillator approximation as[38,41]

$$F^{\text{vib}}_{\text{H}_{\text{ads}}}=\sum_k^{3N_{\text{H}}}\left[\frac{h\omega_k}{2}+k_BT\ln\left(1-e^{\frac{h\omega_k}{k_BT}}\right)\right], \quad (2)$$

where the sum is over the vibrational modes, w_k, of each of the N_i adsorbed hydrogen atoms, H_{ads}. Under those assumptions, it is possible to relate the Gibbs free energy in Eq. (1) to the DFT-calculated energies as[38]

$$G=E_{DFT}+F^{\text{vib}}_{\text{H}_{\text{ads}}}. \quad (3)$$

The other terms in Eq. (1) are the chemical potential of the system components (V_2O_5, O_2, HCl, H_2O, and H_2), which can be experimentally controlled, since they are temperature- and pressure-dependent,[38] as can be seen in Eq. (4),

$$\mu_i\left(T,p\right)=E_i^{\text{total}}\left(DFT\right)+E_i^{ZPE}+\mu_i(T,p^0)+k_BT\ln\left(\frac{p_i}{p^0}\right), \quad (4)$$

where $\mu_i(T,p^0)$ can be obtained form the NIST-JANAF thermochemical tables,[42] at standard pressure p^0, 1 atm; E_i^{ZPE} arises from the zero-point vibrations; and E_i^{total} is the total energy. The relationship between μ_V and μ_O is established through the existence of the V_2O_5 bulk phase in equilibrium with the surface by Eq. (5):

$$\mu_{V_2O_5}\left(T,p\right)=2\mu_V\left(T,p\right)+5\mu_O\left(T,p\right)=g^{\text{bulk}}_{V_2O_5}\left(T,p\right). \quad (5)$$

Both H_2O and H_2 are present in the flue gas so it is possible that either species can act as a hydrogen source or sink depending upon temperature and pressure conditions (i.e., surface condensation or dissociation from the surface). However, for the current application H_2O is considered the only hydrogen reservoir due to the negligible concentration of H_2 present in the flue gas stream. The parameter that determines the formation or dissociation of hydroxyl groups on the V_2O_5 surface associated with either H_2O or H_2 is the oxygen chemical potential.[34,39] If the hydrogen source (or sink, but it is referred to as source throughout) is associated with H_2O then the chemical potential of hydrogen can be written as

$$2\mu_H+\mu_O=\mu_{H_2O}\rightarrow\mu_H=\tfrac{1}{2}(\mu_{H_2O}+\mu_O). \quad (6)$$

If, on the other hand, the hydrogen source is associated with H_2, the chemical potential for hydrogen can be written as

$$\mu_H=\frac{\mu_{H_2}}{2}. \quad (7)$$

Figure 3 is a plot of the hydrogen chemical potentials calculated from these two equations as a function of oxygen chemical potential. This chemical potential is referenced to $1/2E^{\text{total}}_{O_2}$; therefore, $\Delta\mu_O=\mu_O-1/2E^{\text{total}}_{O_2}$. The minimum hydrogen chemical potential governs the nature of the source of hydrogen. As can be seen in Fig. 4, at low values of the oxygen chemical, which is denoted as the oxygen-poor region (OPR), the hydrogen source is H_2. In a coal gasification process the oxygen partial pressure is low, creating a reducing environment in which H_2 is present in a much higher concentration (e.g., 35–45 vol %).[43] For the application of a fuel or syngas, it is likely that the source of hydrogen is from H_2 rather than H_2O. Conversely, for the oxygen-rich region (ORR) at higher values of the oxygen chemical potential, H_2O acts as the hydrogen source. Under flue gas conditions, the O_2 concentration (5%) is large enough to fall into the ORR. For completeness, our analysis will consider the entire range of allowed oxygen chemical potential, with both sources of hydrogen, but with special attention to the chemical behavior in the ORR. It is important to note that since gasification is a reducing environment, the formation of NO_x is low, but still exists and is sourced primarily as a volatile species released from the pore structure of the coal in the gasifier.

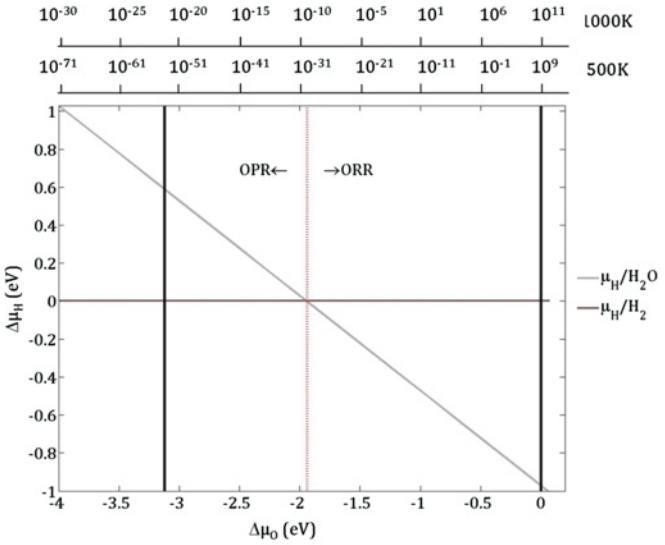

FIG. 3. (Color online) Oxygen regions. The dashed vertical line (at $\mu_O = -1.93$ eV) separates the oxygen-poor region (OPR) from the oxygen-rich region (ORR). Continuous vertical lines (at $\mu_O = -3.12$ and 0 eV) indicate the full range of accessible oxygen chemical potential for V_2O_5. For $\mu_O < -1.93$ eV, μ_H is defined by the equilibrium with H_2 [Eq. (7)] while in the ORR, μ_H is defined by H_2O [Eq. (6)].

Conditions also need to be established for the chlorine source as was done for hydrogen. Under flue gas conditions, the dominant Cl-containing species is HCl with concentrations varying from a few ppm (e.g., Wyodak Bituminous) to several hundred ppm (e.g., North Dakota Lignite),[37] as is shown in Table II. The chemical potential of chlorine can be defined by the following relationship:

$$\mu_H + \mu_{Cl} = \mu_{HCl}. \tag{8}$$

While HCl is the highest source of Cl in the flue gas, its concentration is several orders of magnitude lower than that of H_2O; therefore, its contribution to hydrogen in the gas-phase environment in equilibrium with the surface is likely insignificant. Equation (1) can be rewritten as

$$\gamma = \frac{1}{2A}\left[E_{slab} + F^{vib}_{H_{ads}} - \frac{N_V}{2}E_{V_2O_5} - \left(N_O - \frac{5N_V}{2}\right)\mu_O - N_{HCl}\mu_{HCl} - N_H\mu_H\right], \tag{9}$$

where $E_{V_2O_5}$ is the energy of one V_2O_5 formula unit and μ_H is defined by Eq. (6) or Eq. (7) depending on the oxygen region.

Although the surface is assumed to be in equilibrium with the surrounding environment under all gas-phase conditions, it is necessary to establish physical constraints on the upper and the lower limits of the chemical potential. The lower limit of μ_O is reached when the oxide decomposes into bulk vanadium and gas-phase oxygen, corresponding to the upper value for $\mu_V[g^{bulk}_{V_2O_5}(T,p)]$.[35] Using Eq. (5) the following expression can be derived for the minimum of μ_O:

$$\begin{aligned} \min\mu_O &= \tfrac{1}{5}\left[g^{bulk}_{V_2O_5}(T,p) - 2\max\mu_V(T,p)\right] \\ &= \tfrac{1}{5}\left[g^{bulk}_{V_2O_5}(T,p) - 2g^{bulk}_{V}(T,p)\right]. \end{aligned} \tag{10}$$

The upper limit for the oxygen chemical potential is defined as the value at which oxygen begins to condense on the surface. However, the critical temperature for condensed O_2 solid phase is 150 K, which is below our temperature region of interest; therefore, Reuter and Scheffler[35] suggest defining the upper limit as

$$\max\mu_O(T,p) = \tfrac{1}{2}E^{total}_{O_2}, \tag{11}$$

where E_{O_2} is the total energy of a free, isolated O_2 molecule at 0 K. Rewriting these two oxygen chemical potentials as

$$\tfrac{1}{2}\Delta G_f^{V_2O_5}(0,0) < \mu_O(T,p) - \tfrac{1}{2}E^{total}_{O_2} < 0, \tag{12}$$

$$-3.13\text{ eV} < \Delta\mu_O(T,p) < 0, \tag{13}$$

where $\Delta G_f^{V_2O_5}$ is the difference between the lower [Eq. (10)] and upper limits [Eq. (11)]. The term $\Delta\mu_O(T,p)$ is equivalent to the two last terms on the right-hand side of Eq. (4) and represents the x axis in both Fig. 3 and Fig. 4.

For the case of O_2, it was necessary to carry out spin-polarized calculations to compute accurate energies. It is well known that DFT carries an error in predicting small molecule properties,[34,35] which is the reason why Reuter and Scheffler[35] suggest replacing the oxygen-poor limit energy expression ($1/2E^{total}_{O_2}$) with the potentially more accurate bulk and slab values. We decided to use the direct DFT E_{O_2} value for the lower limit of the oxygen chemical potential, after a rigorous analysis of its associated errors. Previously it was reported,[34,35,44] that $\Delta G_f^{V_2O_5}$ or any oxygen-containing species may be affected by the inherent error in the E_{O_2} term. Under those circumstances, Reuter and Scheffler[35] proposed to use

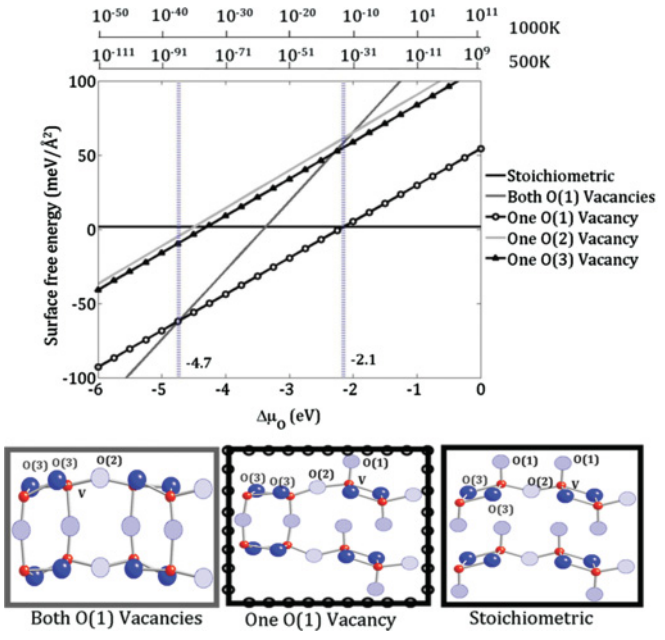

FIG. 4. (Color online) (Top) Thermodynamic stability of three V_2O_5(001) surface terminations under a wide range of partial pressures of oxygen at 500 K and 1000 K. (Bottom) Representation of the most stable structures. The color and style of the outer line of each panel match the color and style of the surface free energy line in the top part of the figure.

experimentally derived values for $\Delta G_f^{V_2O_5}$. One method to assess if the error associated with E_{O_2} cancels out with the error in the V_2O_5 bulk and slab calculations is to compare the experimental value for $\Delta G_f^{V_2O_5}$ with the DFT-calculated value, which for our system is defined as

$$\Delta G_f^{V_2O_5}(0,0) = \left[g_{V_2O_5}^{\text{bulk}}(T,p) - 2g_V^{\text{bulk}}\mu_O(T,p) - \tfrac{5}{2}g_{O_2}^{\text{gas}}(T,p)\right]. \quad (14)$$

Our DFT-calculated value for $\Delta G_f^{V_2O_5}$ only differs by 2.7% from the experimental value (−16.07 eV),[45] which is lower than the 5% difference found in similar DFT studies.[34,35] On the other hand, although our DFT-predicted binding energy for the free O_2 molecule (−6.04 eV) is higher than that of experiment[45] (−5.16 eV), it is in reasonable agreement with DFT studies carried out previously.[14,44,46] Mason *et al.*[34] observed that by adding a correction term ($E_{O_2}^c$) to the DFT-derived E_{O_2} term, they were able to get closer to the experimental value of $\Delta G_f^{V_2O_5}$. This correction term was computed by comparing DFT and experimental atomization energies. Although we calculate the same correction term, negligible improvement was obtained by its addition to the DFT-derived $E_{O_2}^{\text{total}}$ term. This analysis supports our approach of using the direct DFT-derived E_{O_2} value for the lower limit of the oxygen chemical potential.

III. RESULTS AND DISCUSSION

A. Optimization of stoichiometric V_2O_5(001) surface

To optimize the computational time and accuracy in simulating the (001) surface, one-layer, two-layer, three-layer, and five-layer-slabs were tested. In general, accuracy is reached when the bond distance in the inner layers does not change with respect the bulk configuration. The layer spacing of the bulk, two-layer, and five-layer slabs and percent difference between the layers with respect to the bulk was calculated and negligible changes (<1%) in those distances were observed in any of the simulated slabs, which suggested that V_2O_5(001) surface exhibits very bulklike behavior with a weak interlayer interaction due mainly to van der Waals forces.[23,29,31] The energy per formula unit of each slab was compared with the that of the five-layer slab to determine the effect of the number of layers on this value. The energy difference between the two-layer and five-layer slabs was only 0.02%, which also supports the use of a two-layer-slab to simulate the V_2O_5(001) surface, thereby limiting computational expense. Our literature review reveals that one- or two-layer-slabs are generally adequate to simulate the (001) surface.[14–16,23,24,29,31,33]

The electronic characterization of the V_2O_5(001) surface has been carried out using a DOS and Bader charge analysis. DOS of the V_2O_5(001) surface showed clear similarities in the band structure with the bulk, further showing the bulk-like behavior of this surface. The Bader charge analysis allows for the estimation of the charge distribution by considering the charge enclosed within the Bader volume as an approximation to the total electronic charge associated with a given atom.[47] The charge distribution of bulk V_2O_5 indicates that the O(1) atoms withdraw less charge from vanadium than the O(2) and O(3) atoms. In Lewis acid-base terms, this implies that the O(1) site has less Lewis-base character since it has less charge to donate compared to the O(2) and O(3) sites. This is consistent with Pauling-scale electronegativities[45] of O(3.44) and V(1.63). The higher the number of neighboring vanadium atoms an oxygen atom has, the more electron density it withdraws, leading to a stronger Lewis base with increased charge to donate. This acid-base chemistry across the catalyst surface can provide intuition on how Hg^0 may oxidize. The Hg^0 oxidation across this system would require Hg to interact with a site that has the capability of withdrawing electron density, oxidizing Hg^0 to Hg^{2+}. From this analysis, the weaker Lewis base sites associated with the O(1) atoms would be more likely to oxidize Hg^0, consistent with the Pauling-scale electronegativity of Hg(2.00).

B. Oxygen vacancies

Several studies proposed[2,15] that Hg oxidation over V_2O_5 involves the extraction of a lattice oxygen, leaving oxygen vacancies behind which are replenished from the gas phase, via a Mars-Maessen mechanism. On the other hand, Göbke *et al.*[19] suggests that adsorption/dissociation of methanol leading to adsorbed methoxy and hydroxy groups only takes place in the presence of vanadyl defects since the stoichiometric surface is unreactive for this reaction. Since vanadyl oxygen vacancies play an important role in the reactivity of V_2O_5(001) surface for those reactions, it is important to analyze the stability of the partially reduced V_2O_5(001) surfaces under flue gas conditions as a function of the oxygen partial pressure and temperature to understand the function of this oxide as a catalyst for mercury oxidation.[14]

The thermodynamic stabilities of four reduced structures are compared to the stoichiometric surface at 0 K in Fig. 4. It is possible to see that the O(1) vacancies are more stable than the O(2) or O(3) vacancies for any range of chemical potential of oxygen. These results are in agreement with previous studies of Goclon *et al.*,[15] in which they showed a smaller energy requirement for the formation of the O(1) vacancy compared to the other two oxygen vacancies, suggesting this vacancy to be the most likely. The results of the *ab initio* thermodynamics presented in Fig. 4 can be also be represented as a phase diagram as demonstrated in Fig. 5. This diagram provides additional intuition into the experimentally accessible (T,p) conditions that lead to stable configurations. The phase diagram is created by choosing the most stable structure at each (T,p) condition.[38] Under flue gas conditions (300 K < T < 1000 K, $p_{O_2} \approx 0.05$ atm), the stoichiometric surface is the most stable structure.

These results are supported by STM experimental results from Blum *et al.*,[33] who suggest that vanadyl oxygen atoms desorb from the surface at 800 K, yielding an oxygen-deficient surface under ultra-high-vacuum conditions (base pressure = 2×10^{-13} atm, $p_{O_2} \approx 4.2 \times 10^{-15}$ atm). Only under extreme cases of low oxygen concentration or high temperature is it possible to obtain reduced surfaces of unsupported V_2O_5. Work done by Busca *et al.*[17] using FT-IR spectroscopy on unsupported V_2O_5 presented it as an oxygen-vacancy-free material. Furthermore, work by Gobke *et al.*[19] suggests that the energy requirements for the production of vanadyl oxygen vacancies is so high that it prevents those vacancies from being

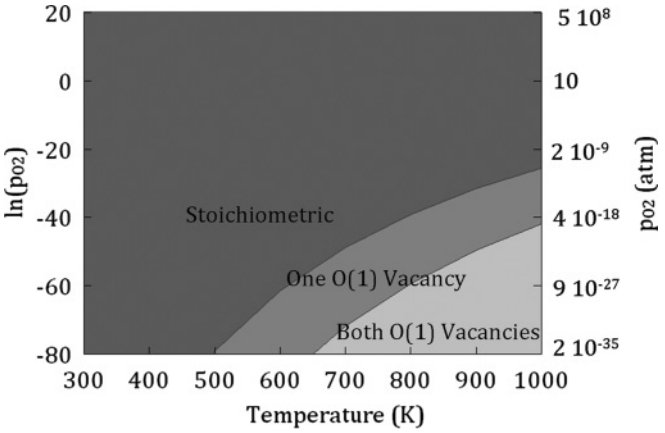

FIG. 5. Temperature and p_O phase diagram of oxygen vacancies on V_2O_5.

created by thermal treatment of the surface. In future work, it will be useful to investigate the Hg oxidation mechanism associated with the O(1) atom, leading to the O(1) vacancy that is predicted to be the most stable in accordance with the *ab initio* thermodynamics predictions.

The current results of the surface relaxation investigation corroborates previous findings[14,15,48] which showed that the largest structural change associated with the vacancy formation is the decrease of the interlayer distance, with the creation of bonds between the V atom and O(1) atom from the first and second layers. The average layer distance for the stoichiometric, one O(1) vacancy, and both O(1) vacancies structures are 4.82, 4.37, and 4.22 Å, respectively, with 9.03% and 12.14% layer contraction for the two latter cases. The formation of the interlayer bonds and the subsequent surface relaxation was described for the first time by Ganduglia-Pirovano and Sauer[14] as the main driving force for the defect formation. When oxygen atoms are removed from the surface, two electrons are left behind which get distributed over the closer V atoms. Those V atoms are more ready to react with neighboring O(1) atoms leading to this interlayer interaction.[33,48] On the other hand, a study by Brazdova *et al.*[29] showed that this surface relaxation due to the interlayer V–O–V interaction does not take place for epitaxial vanadium oxides films supported on Al_2O_3 (same composition as V_2O_5 but different coordination). The facility to create oxygen vacancies is influenced by this surface relaxation so the role of oxygen vacancies on the oxidation mechanism will depend on the effect of the support. As Sauer *et al.*[48] reported in their work, the dissociation energy of the V = O(1) bond decreases from 286 kJ mol^{-1} to 113 kJ mol^{-1} due to the surface relaxation. A more detailed geometry analysis is shown in Fig. 12 in the Appendix.

The DOS for the single- and double-vacancy structures are compared with stoichiometric surface and it showed a decrease in the original band gap from 1.78 eV in the stoichiometric surface to 1.67 eV in the single O(1) vacancy surface and 0.78 eV in the double O(1) vacancy structures. Both the broadening of the conduction band and the decrease of the band gap were reported experimentally by Blum *et al.*[33] using STM in what they refer to as a surface semiconductor-to-metal transformation. A more detailed analysis and the plot of the DOS is shown in Fig. 13 in the Appendix.

C. Surface protonation and hydroxylation

1. Thermodynamic stability

The presence of H_2O, and to a very small extent H_2, in the flue gas, may lead to the V_2O_5(001) surface terminated by hydrogen and hydroxyl groups that could modify the functionality of the oxide. Special attention is paid to the interaction of the V_2O_5(001) surface with H_2O since the oxygen concentration in the flue gas corresponds to the ORR, which is defined by the equilibrium with H_2O, as was shown in Fig. 3. Two cases were tested.

(i) The first case consists of the OH/H terminated surfaces where n is the total number of H_2O molecules adsorbed and dissociated on surface oxygen atoms. We refer to the stoichiometric surface as $V_{2m}O_{5m}$ and structures are named as $nH_2O \times [V_{2m}O_{5m}]$ following a specification of the adsorption sites (e.g., $H_2O \times [V_{2m}O_{5m}]$: H–O(1),OH–V means that H is adsorbed on a O(1) atom and OH on a V atom of the stoichiometric surface). An example of these surfaces is shown in Fig. 6.

(ii) The second case consists of the H-terminated surfaces, where n is the total number of H atoms adsorbed on surface oxygen atoms. These structures are named as $nH \times [V_{2m}O_{5m}]$ following a specification of the adsorption sites (e.g., $H \times [V_{2m}O_{5m}]$: H − O(1) means that H is adsorbed on the O(1) in the stoichiometric surface). Selected examples of these surfaces are shown in Fig. 7.

A total of 20 surfaces with either OH/H or H groups interacting with different surface atoms were tested; however, only the structures with the lowest surface free energies are shown in Figs. 6 and 7, while detailed information regarding the others is available in Figs. 14 and 15 in the Appendix.

The thermodynamic stability of the different protonated and hydroxylated surfaces calculated at 0 K for the allowed range of oxygen chemical potential is shown in Fig. 14.

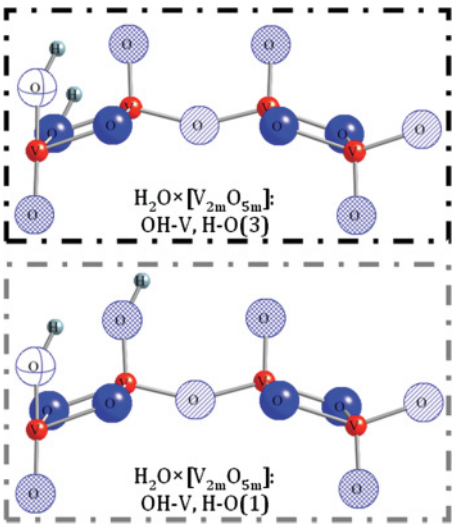

FIG. 6. (Color online) Two possible hydroxylated surfaces where an OH–group (white atom with blue equatorial line is O and small gray atoms are H) is adsorbed onto a V atom (small red atom) and an H–atom (gray atom adsorbed onto any of the oxygen surface atoms [O(1), O(2), or O(3)]. The color and style of the outer lines of the panels match the color and style of the respective surface free energy lines in Fig 7.

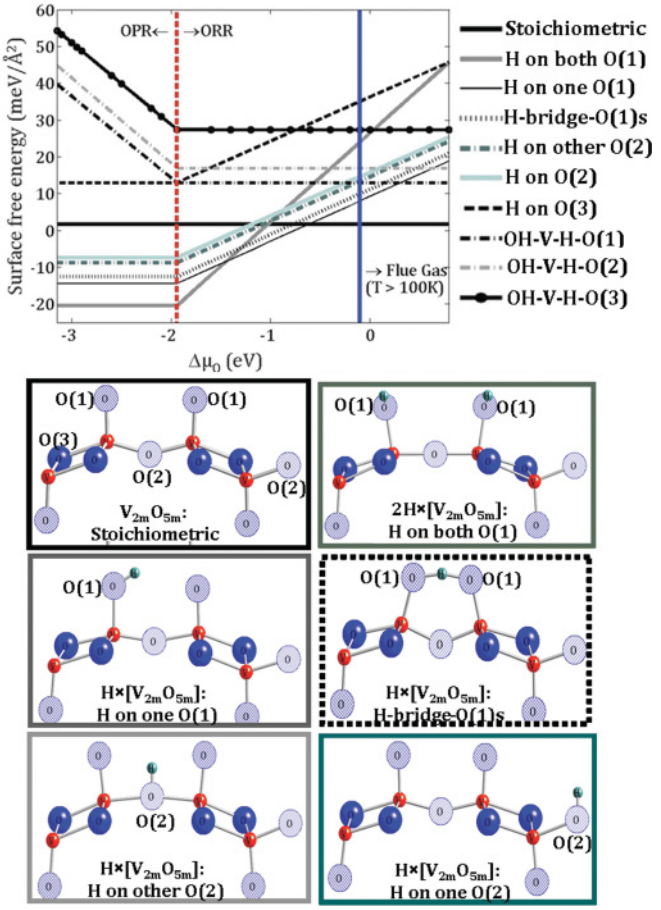

FIG. 7. (Color online) (Top) Surface free energy as a function of oxygen chemical potential for different protonated and hydroxylated surfaces over the full range of accessible $\Delta\mu_O$ (−3.12 and 0 eV). (Bottom) Examples of the most stable protonated surfaces. The color and style of the outer lines of the panels match the color and style of the respective surface free energy lines in the top part of the figure.

The remaining gas components are fixed at the flue gas conditions for lignite coal combustion [H_2O (9.27 wt%), HCl (136.9 ppm), H_2 (although negligible for combustion applications, we assumed 1 ppb to solve the surface free energy equation in Eq. (9)].[37]

In Fig. 7, the two oxygen regions are separated by the vertical red dotted line at $\mu_O = -1.94$ eV. As previously mentioned, the region on the left is the OPR, where μ_H is determined by the equilibrium with H_2 while in the ORR, μ_H is determined by availability of H_2O. Surface protonation seems to be favored when H_2 is in equilibrium with the surface in the OPR; however, in the ORR the protonated surfaces have higher surface free energies, leading to the stoichiometric surface as the most stable structure. The change in hydrogen source leads to a change in the slope. Only three structures are stable over the entire range of accessible μ_O, that is, the structure in which both of the O(1) atoms are protonated, the structure in which one O(1) atom is protonated, and the stoichiometric surface. Paying attention to the region close to the flue gas conditions, both the single O(1)–H and single H–bridge O(1)*s* structures have similar surface energies, making it difficult to distinguish between the more stable one since their energy difference falls

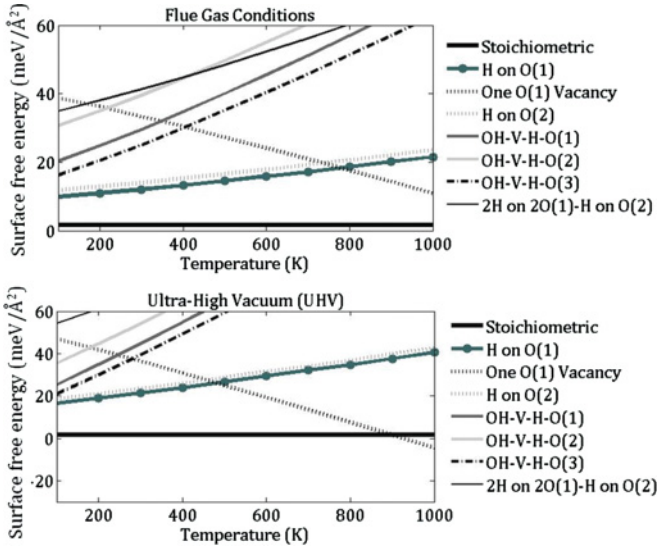

FIG. 8. (Color online) Surface free energies as a function of temperature for various H- and OH-terminated surfaces under (top) flue gas conditions and (bottom) UHV.

within the error of DFT, resulting in the potentials of both structures being stable. The most stable protonated surfaces are those in which the H atoms interact with the O(1) atoms. The higher reactivity of this oxygen atom has been shown in previous studies.[14,22,24] The Bader charge analysis showed that O(1) atom withdraws fewer electrons from the neighboring V atom, making it the weaker base, but still more electronegative than hydrogen. The other two oxygen atoms, O(2) and O(3), are strong Lewis bases so they will not react as easily with hydrogen, which is an electron donor in its atomic state.

The region to the right of the second vertical line blue at $\mu_O = -0.1$ eV corresponds to flue gas conditions (or conditions at the SCR) for all temperatures above 100 K. Within this region neither H- nor OH-/H-terminated surfaces are stable. Our results agree with the *in situ* experiments by Tepper *et al.*,[16] who also found no stable hydroxylated surfaces at similar conditions. The Tepper *et al.* study suggests that the interaction of atomic hydrogen with the surface is not thermodynamically stable. Therefore, we can conclude that the presence of H_2O and H_2 in the flue gas will not modify the geometry and composition of the $V_2O_5(001)$ surface at the SCR conditions. It is important to note that in a reducing gasification environment it is likely that the V_2O_5 surface will be protonated, which will influence its catalytic reactivity for these applications.

The stability of the protonated surfaces is compared with results of ultra-high-vacuum (UHV) experiments, in a similar manner to the work carried out by Mason *et al.*[34] Since the conditions employed in the majority of the spectroscopy techniques used for surface characterization on experimental studies require UHV conditions, it is important to analyze the thermodynamic stability under these conditions for additional benchmarking of our theoretical predictions. The thermodynamic stability of the surfaces investigated in the present work as a function of temperature (100 K–1000 K) under flue gas composition conditions in addition to UHV conditions ($p_{O_2} = p_{H_2O} = p_{HCl} = 10^{-10}$ atm) is shown in Fig. 8.

TABLE III. Comparison of the adsorption energies using atomic and molecular gas-phase (inside parentheses) hydrogen as a reference on various oxygen sites of the (001) surface (eV).

Source	O(1)	O(2)	O(3)
Present work	−2.95 (−0.66)	−2.66 (−0.38)	−1.78 (0.48)
Goclon *et al.*	−2.97	−2.71	−2.42

We can conclude from Figs. 7 and 8 that the stoichiometric surface is the most stable structure for any temperature under flue gas conditions. However, at high temperatures under UHV conditions, the V_2O_5(001) surface becomes partial reduced. The bottom graph of Fig. 8 shows that the single O(1) vacancy becomes the most stable structure at temperatures above 900 K. These results are supported by our previous phase diagram (Fig. 5), which showed that at these conditions (900 K and $p_{O_2} = 10^{-10}$ atm), the presence of a single O(1) vacancy is the most stable structure.

Our *ab initio* thermodynamic results suggest that the V_2O_5(001), under flue gas conditions, does not react with either H_2O or H_2, even at low temperatures. These results at first glance appear to contradict the previous work of Goclon *et al.*,[15] where they obtain negative adsorption energies for atomic H on the different oxygen atoms of the (001) surface [referenced as the (010) surface in Goclon *et al.*[15]]. However, these adsorption calculations are performed using direct DFT-derived energy results which imply that the adsorption occurs at 0 K. In their work, they calculated adsorption energies for atomic hydrogen on the surface with the equation

$$E_{\text{ads}}(\text{H}) = E(\text{V}_{2m}\text{O}_{5m}\text{H}) - E(\text{V}_{2m}\text{O}_{5m}) - E(\text{H}), \quad (15)$$

where E(H) is the energy of an isolated hydrogen atom, $E(\text{V}_{2m}\text{O}_{5m})$ is the stoichiometric surface, and $E(\text{V}_{2m}\text{O}_{5m}\text{H})$ is the total energy of the protonated surface. However, the current work has been carried out in the context of *ab initio* thermodynamics in which one source of atomic H is H_2 and defined by

$$E(\text{H}) = \tfrac{1}{2}E(\text{H}_2). \quad (16)$$

With the purpose of verifying our methodology and *ab initio* predictions, we compare our adsorption energies using both atomic and molecular gas-phase hydrogen with the results of Goclon *et al.*[15] The results for the $1 \times 1 \times 1$ unit cell (referenced as the small supercell in Goclon *et al.*) are presented in Table III.

As can be seen from Table III, our adsorption energy predictions are in reasonable agreement with those of Goclon *et al.*[15] and certainly follow the same trend, with O(1) being the strongest site for hydrogen adsorption and O(3) the weakest. The difference between our values and Goclon *et al.* could be due to the way in which the systems were defined. In our case a symmetric slab with a double vacuum region is used with opposing dipoles on either side of the slab canceling with periodic images, while Goclon *et al.* only use a single-sided slab, with no mention of dipole corrections. The way in which we assume the energy of atomic hydrogen energies may also differ. In the current work, we calculated the total energy of atomic H based upon a spin-polarized state following the work of Kresse.[49] The most important information that can be extracted from Table III is that in the case of the calculated adsorption energy using molecular hydrogen as a reference, the values are dramatically smaller than the case in which molecular hydrogen is used as a reference. Furthermore, the interaction of molecular H with the O(3) atom becomes energetically unfavorable. These small adsorption energies correspond to weakly adsorbed atomic hydrogen, which can easily desorb from the surface with an increase in temperature.

2. *Surface relaxation*

By analyzing the structural and electronic properties of the next-most-stable protonated structures besides the stoichiometric surface in the region close to flue gas conditions, we can understand how water vapor may influence the surface reactivity of this oxide. In Fig. 9 we show bond and interlayer distances of the two next most stable protonated surfaces. The changes in these distances with respect the stoichiometric surface are shown in parentheses.

There is an elongation of the V–O(1) bond when this oxygen is interacting with atomic H, along with small changes in the bond distances of the in-plane oxygen atoms, O(2) and O(3). Similar effects were also observed by Goclon *et al.*,[15] although the changes in these bond distances were slightly different possibly because they protonated only one side of their slab. There is a possible correlation between the elongation of the V–$O(1)^H$ bond with a layer contraction (average distance marked

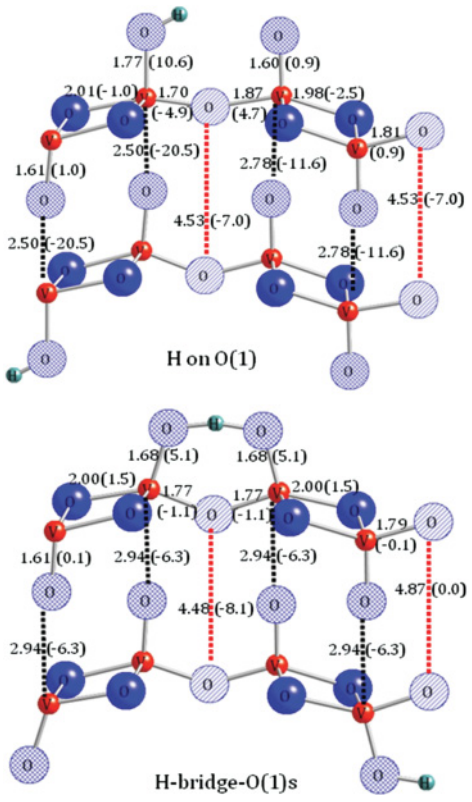

FIG. 9. (Color online) Bond and interlayer distances for the two more stable hydrated surfaces close to flue gas conditions. Changes with respect to the stoichiometric surface are shown inside the parentheses.

by red dotted lines in Fig. 9). In the case of the one O(1)–H structure, the bond V–O(1)^{H} is elongated by 10% with a layer contraction of 9.39%. While in the case of the one H–bridge O(1)*s* structure, the same distance is only elongated by 5% with a layer contraction of 5.29%. The longer the V–O(1)^{H} distance, the larger is the layer contraction. This phenomenon is correlated with the layer contraction observed within the partially reduced surfaces in which the V–O(1) distances were stretched to the point of cleavage, leaving behind an oxygen vacancy and yielding a strong contraction of the interlayer spacing.

3. *Density-of-states analysis*

The adsorption of atomic H results in changes in the electronic structure of the V_2O_5(001) surface. This is illustrated in Fig. 10 by the electronic DOS of the stoichiometric and the previous protonated surfaces. The surface relaxation upon protonation leads to a shift in the conduction band below the Fermi level, which is an effect also observed upon the formation of vacancies. In the case of oxygen vacancies, two extra electrons remained at the vacancy site per oxygen atom removed, splitting the V 3*d* states and broadening the conduction band. For the protonated surfaces, the donation of electrons by the hydrogen atoms produces decreased broadening of the conduction band since the excess electrons surrounding the protonated V atom are also less. The peak overlap between the O(1) atom and H atoms occurs at a low energy (−20 eV) for the case of H on O(1) structure, while the main H peak overlap occurs at a higher energy (−7.5 eV) in the case of the H–bridge–O(1)*s* structure. In general, when peaks shift to lower energies, it is an indication of increased stability. Thus, the fact that the peak overlap between the H and O(1) atoms for the single O(1)–protonated surface structure is at a lower energy than that of the one H–bridge–O(1)*s* structure, suggests a higher stability of the former structure. The distinction between these two structures based only on their surface free energy was not possible because of the small difference in their energy values falls within the DFT error. By using DOS analysis was it possible to conclude that the single O(1)–protonated structure is more stable than H–bridge–O(1)*s*.

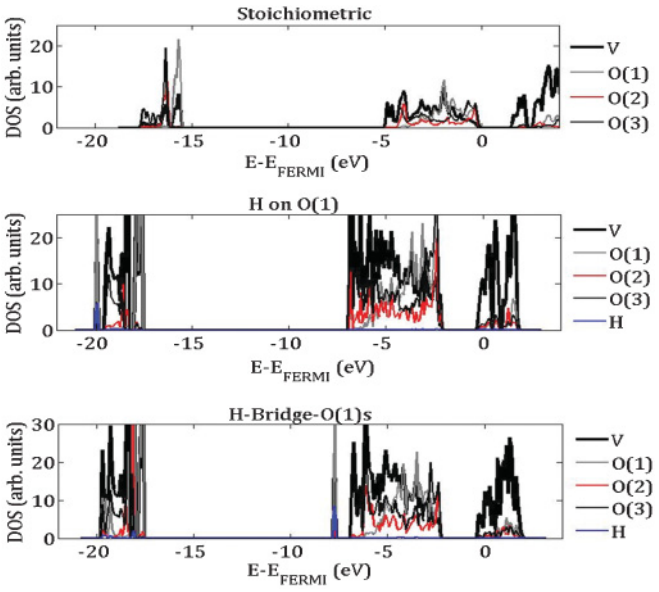

FIG. 10. (Color online) DOS of stoichiometric H on O(1) and H–bridge–O(1)*s* structures. DOS energies are referenced to the calculated Fermi level.

D. Chlorinated surfaces

The presence of HCl in the gas phase may lead to surface chlorination under flue gas conditions. The role of HCl during Hg oxidation is still unclear. While some authors suggest the direct interaction of HCl with the oxide surface, followed by an interaction with the Hg present in the flue gas (Niska and Fujiwara[6]), others suggest that Hg directly reacts with the oxide surface and it is later oxidized by HCl present in the gas phase (Senior and Linjewile[5]). Analyzing the stability of different chlorinated structures may help to clarify the role of HCl during Hg oxidation. The stability of chlorinated surfaces is investigated by simulating the interaction between Cl and H atoms with the three nonequivalent surface oxygen atoms. Only surfaces with adsorbed Cl and H atoms have been simulated, which allows us to simplify the expression for the surface free energy, since we can assume that both Cl and H atoms are sourced from HCl and not from H_2O. Similar to the previous discussion, the remaining gas compositions are fixed at flue gas conditions, that is, H_2O (9.27 wt%), O_2 (4.65%).[37] Surfaces with a combination of H, OH, and Cl species are not presented in this work. An example of the surfaces simulated and the thermodynamic stability of the all chlorinated surfaces tested are shown in Fig. 11. As can be seen two cases were proposed.

(i) The first type consists of structures where Cl is adsorbed on an O(1) vacancy and the H atom can be adsorbed on the neighbor O(1), O(2), or O(3) atoms. Those surfaces are named as HCl × [$V_{2m}O_{5m-1}$] followed by a specification of the adsorption sites.

(ii) The second type consists of structures where Cl is adsorbed on an O(1) atom and the H atom interacts with the neighbor O(1), O(2), or O(3) atoms. Those surfaces are named as HCl × [$V_{2m}O_{5m}$] followed by a specification of the adsorption sites.

The region on the left of vertical red dotted line in Fig. 11 indicates flue gas conditions [i.e., H_2O (9.27%), HCl (136.9 ppm), O_2 (5%)][37] at any temperature above 100 K. The stoichiometric surface represents the lowest surface free energy, becoming the most stable structure under flue gas conditions at all temperatures considered. Although previous experimental studies[6–8] suggested an interaction between HCl and V_2O_5 present in the SCR catalyst, these studies were performed on supported and well-dispersed V_2O_5 catalyst systems, instead of single-crystal V_2O_5, which is very difficult to obtain experimentally, but is possible by using floating zone melting instead of vapor deposition.[50] The stoichiometric surface is a surface terminated with vanadyl groups which are unreactive. Another possible explanation for the lack of stable chlorinated surfaces could be the low concentration of HCl present in the flue gas (ppm level), since it can be seen in Fig. 11 at 500 K an unreasonably high HCl concentration (10^{18} atm) is required to obtain the first stable chlorinated surface under these coverage conditions (one HCl molecule in

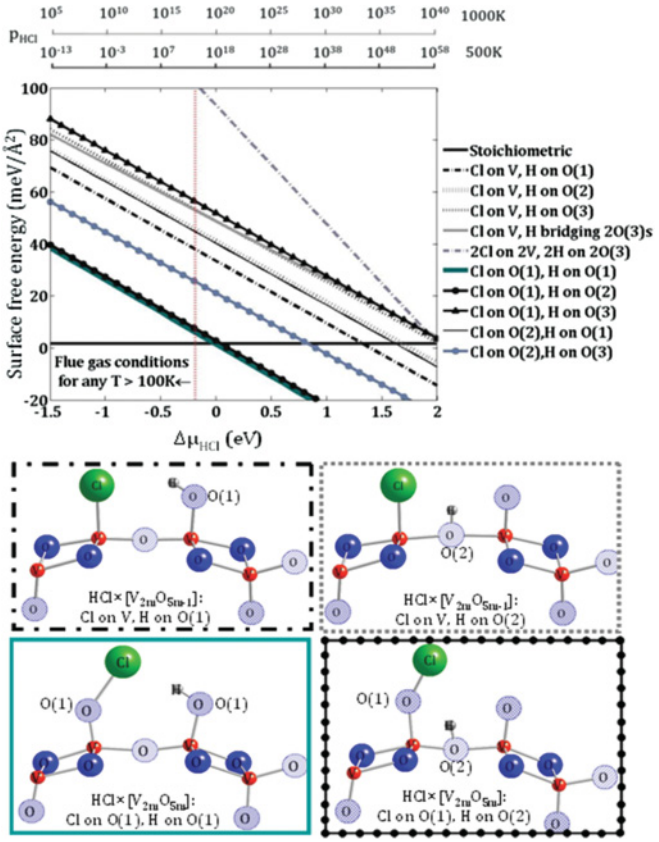

FIG. 11. (Color online) Thermodynamic stability of the chlorinated structures with the lowest surface free energy.

a 1×1 unit cell). As discussed previously, the direct screening approach[38] used in this work indicates that our predictions are restricted to the number of configurations tested. A larger unit cell and higher HCl concentrations could lead to differences in predicted surface stabilities. We did a simple calculation of the area required to obtain a stable chlorinated surface at 500 K with the flue gas conditions described in Table II for the most stable chlorinated surface, that is, Cl with O(1) and H with O(1). In order to be stable, the chlorinated surface needs to have an equal or lower surface free energy than the stoichiometric surface (1.66 meV/Å^2). Keeping this in mind and using Eq. (9), we obtain that the unit cell of the chlorinated surface needs to be 19 times larger than the current unit cell (1×1) to equal the surface free energy of the stoichiometric surface. Due to computational expense and time limitations, surfaces of this size were not simulated.

This thermodynamic study shows that under the flue gas and coverage conditions tested the concentration of HCl is too small to obtain stable chlorinated structures. A better approach, which will be carried out in future work, is to employ reaction path analysis to investigate different chlorine-surface interactions directly. To complement the *ab initio* thermodynamic study, formation energies of the most stable chlorinated surfaces have been calculated using direct DFT-derived energies and the following equation:

$$E_{\text{ads}}(\text{HCl}) = E(\text{V}_{2m}\text{O}_{5m}\text{HCl}) - E(\text{V}_{2m}\text{O}_{5m}) - E(\text{HCl}), \quad (17)$$

where E(HCl) is the energy of an isolated gas-phase HCl molecule, $E(\text{V}_{2m}\text{O}_{5m})$ is the stoichiometric surface, and $E(\text{V}_{2m}\text{O}_{5m}\text{HCl})$ is the of the chlorinated surface. Those formation energies are an approximation since they do not take into account the energy required to dissiociate HCl into H and Cl atoms. Those formation energies of the chlorinated surfaces shown in Fig. 11 are presented in Table IV.

As can be seen from Table IV, for the conditions tested, only one chlorinated surface has a favorable formation energy [Cl adsorbed on the O(1) atom and H adsorbed on the neighboring O(1) atom]. However, this formation energy is small, which means that with an increase in temperature the H and Cl atoms from HCl molecules desorb easily from the surface. From Table IV and Fig. 11 we can conclude that the Cl atom prefers to interact with the surface atoms instead of directly with a V atom (available due to a oxygen vacancy). Furthermore, we can conclude that the interaction between the O(1) and Cl atoms is more stable than the interaction with O(2) with an energy difference of 1.64 eV. It seems that among the surface oxygen atoms, the O(1) is the most reactive toward both H and Cl atom interactions. This higher reactivity of the vanadyl atoms is also supported by previous studies about the interaction with H atoms.[14,15,21]

Bench-scale experiments in addition to pilot-scale testing verify that Hg to some extent is indeed oxidized across the SCR catalyst. Although the majority of the V_2O_5 catalysts used in SCR units are prepared by vapor deposition on an oxide support (e.g., TiO_2 or Al_2O_3), the effect of the support was not taken into account in the current study because we wanted to isolate the individual contribution of the V_2O_5 catalyst to the SCR reactivity. It is assumed that vanadium strongly interacts with the metal oxide support due to the high heat of formation of vanadium oxides.[51] When TiO_2 is used as a support, it is reduced by vanadium due to the high affinity of vanadium for oxygen,[52] so the degree of oxidation of the V_xO_y oxide depends on the accessibility of oxygen atoms from the support and/or gas-phase environment to the vanadium oxide formation. Also, it is likely that the highly dispersed[8] vanadia catalyst restructures upon dispersion onto the support or there exists an increase in defect sites upon deposition, which may also lead to phase transformations and potential increased reactivity.[33] For example, for V_2O_5 supported on Al_2O_3, the V = O bond dissociation energies are higher since the surface relaxation associated with the creation of those vacancies in a unsupported V_2O_5 does not occur when Al_2O_3 is used as a material since the V–O–V interlayer interaction does not take place.[48]

IV. SUMMARY

The structural and electronic changes on the V_2O_5(001) surface under flue gas conditions were analyzed upon vacancy formation, hydroxylation, and chlorination. Under the flue gas environment and coverage conditions tested, the stoichiometric surface was found to be the most stable structure. Our analysis of the thermodynamic stability of structures with oxygen vacancies as a function of oxygen partial pressure showed that structures with vacancies of one or two vanadyl oxygen atoms [i.e., O(1)] were the most stable of all the partially reduced surfaces tested.

TABLE IV. Formation energy of different chlorinated surfaces in (eV).

HCl × $[V_{2m}O_{5m-1}]$	Energy (eV)	HCl × $[V_{2m}O_{5m}]$	Energy (eV)
Cl on V, H on O(1)	6.261	Cl on O(1), H on O(1)	−0.015
Cl on V, H on O(2)	6.618	Cl on O(1), H on O(2)	0.043
Cl on V, H on O(3)	6.949	Cl on O(1), H on O(3)	2.079
Cl on V, H bridging O(3)*s*	7.056	Cl on O(2), H on O(1)	1.625
2Cl on V, 2H on O(3)*s*	7.781	Cl on O(2), H on O(3)	0.834

In agreement with previous work, the interaction of the $V_2O_5(001)$ surface with H_2O and H_2 indicated that the O(1) atoms were the most reactive surface atoms. Structures with a single O(1) atom protonated became stable under more humid conditions; thus, the stoichiometric surface remains the most stable structure under coal-fired oxidized flue gas conditions. There is slight contraction of the interlayer distances and a smaller broadening of the conduction band below the Fermi level compared to the vacancy case due to a decreased electron accumulation.

The thermodynamic stability analysis of several chlorinated surfaces showed that none of those surfaces are stable under flue gas conditions for the coverage tested. Larger HCl concentrations or smaller coverages may lead to stable chlorinated structures; however, the computational expense of these calculations was too great to carry this work out. The analysis of the formation energy of several chlorinated surfaces showed that only the interaction between the vanadyl oxygen, O(1), with Cl has a small but favorable energy. The other chlorinated structures tested showed positive formation energies which make them unfavorable. This analysis also showed that Cl prefers to interact directly with surface oxygen atoms, instead of V atoms which could be available through the presence of oxygen vacancies.

In addition to the catalyst support interactions and effects from vanadia dispersion on the support, the reactivity of the V_2O_5 catalyst could also be in part due to geometrical and electronical changes created in the reactivity of V_2O_5 supported on TiO_2 and its stability under flue gas conditions. Additionally, reaction path analysis will be employed to determine likely pathways of trace metal oxidation with reactive vanadia surfaces.

ACKNOWLEDGMENTS

This work was supported by Fundacion Caixa Galicia scholarship for graduate studies and the Stanford University School of Earth Sciences Graduate Fellowship Program. Computational resources were provided by Stanford's Center for Computational Earth and Environmental Science (CEES) and the authors gratefully acknowledge the assistance of CEES systems administrator, Dennis Michael.

APPENDIX

A. Surface relaxation of the partial reduced surfaces

The effect of the single oxygen vacancy on the surface relaxation is investigated by analyzing the change in layer spacing with respect the stoichiometric surface, as shown in Fig. 12.

The average layer-spacing distances for the stoichiometric single O(1) vacancy and both O(1) vacancies structures are 4.82, 4.37, and 4.22 Å, respectively, with a 9.03% and 12.14%

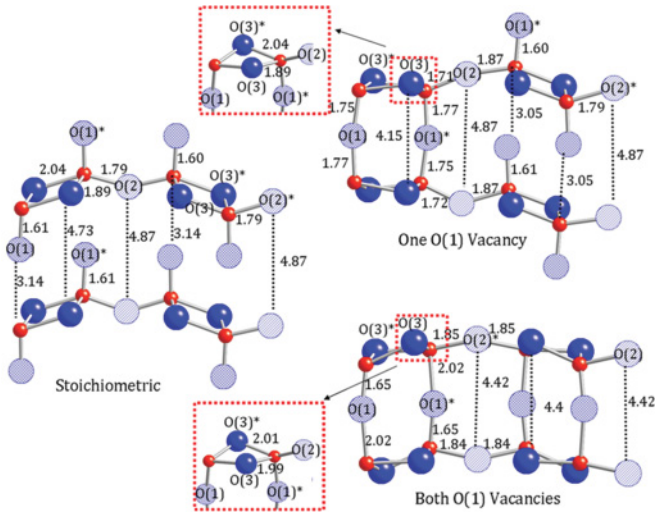

FIG. 12. (Color online) Representation of the stoichiometric and single O(1) vacancy. The small dotted square helps to show the V–O(3) and V–O(3)* bond distances. The vertical dotted lines assist in determining the changes in the interlayer distances.

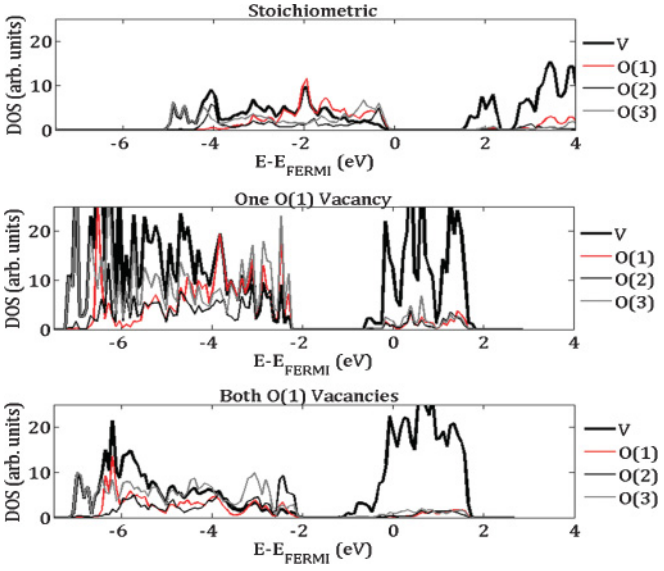

FIG. 13. (Color online) Comparision of DOS of stoichiometric one O(1) vacancy and both O(1) vacancies surfaces. All DOS energies are referenced to the calculated Fermi level.

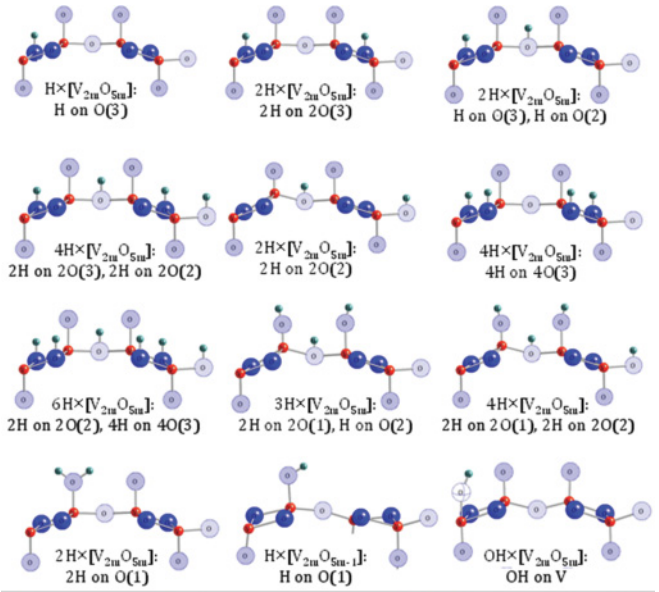

FIG. 14. (Color online) Thermodynamic stability of the hydroxilated/protonated surfaces tested in this works that were not included in the main text.

layer contraction for the two latter cases. The presence of a single O(1) vacancy causes a strong, but only local, distortion of the atomic structure, while in the case of both O(1) vacancies it results in a much smaller structural distortion but one that affects the whole structure.

B. Density-of-states analysis of partial reduced surfaces

DOS calculations have been performed to understand the change in the electronic structure of the surfaces with O(1) vacancies, since these are predicted to be the most stable partially reduced surfaces. Using the stoichiometric surface as a reference, the DOS for the single- and double-vacancy structures are compared in Fig. 13.

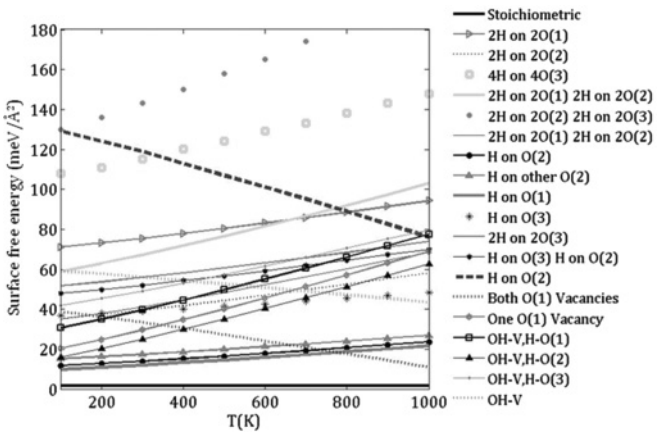

FIG. 15. Other hydroxylated/protonated surfaces tested.

The bulklike character of the stoichiometric surface is evident at the top of Fig. 13, indicating an indirect band gap of 1.78 eV. After the removal of neutral oxygen atoms,[14] two electrons are left behind at each vacancy site, creating an excess of electrons that lead to a split of the V 3*d* states, which further leads to a broadening of the conduction band below the Fermi level. There is a decrease in the original band gap from 1.78 eV in the stoichiometric surface to 1.67 eV in the single O(1) vacancy surface and 0.78 eV in the double O(1) vacancy structures. In the case of the two latter structures, we call band gap, which is the gap between the former valence and conduction bands. The removal of additional oxygen atoms results in increased broadening of the conduction band, which further decreases the band gap.

C. Stability of other protonated/hydroxilated surfaces tested

Figures 14 show all the additional protonated and hydroxylated surfaces tested, which were not shown previously in the main paper. Figure 15 shows the thermodynamic stability of all protonated and hydroxylated surfaces tested in this work.

*wilcoxj@stanford.edu

[1]United States Environmental Protection Agency, *Environmental Footprints and Cost of Coal-Based Integrated Gasification Combined Cycle and Pulverized Coal Technologies*, EPA-430/R-06/006 (EPA, 2006).
[2]A. A. Presto and E. J. Granite, Platinum Met. Rev. **52**, 144 (2008).
[3]H. Kamata, S. Ueno, T. Naito, and A. Yukimura, Ind. Eng. Chem. Res. **47**, 8136 (2008).
[4]A. A. Presto and E. J. Granite, Environ. Sci. Tech. **40**, 5601 (2006).
[5]C. L. Senior and T. Linjewile, *DOE/NETL Mercury Control Technology R&D Program Review* (National Energy Technology Laboratory, Pittsburgh, 2004).
[6]S. Niksa and N. Fujiwara, J. Air Waste Manage. Assoc. **55**, 1866 (2005).
[7]Y. Eom, S. H. Jeon, T. A. Ngo, J. Kim, and T. G. Lee, Catal. Lett. **121**, 219 (2008).
[8]S. He, J. S. Zhou, Y. Q. Zhu, Z. Y. Luo, M. J. Ni, and K. F. Cen, Energy Fuels **23**, 253 (2009).
[9]T. Oshio, Y. Sakai, T. Moriya, and S. Ehara, Scanning Microsc. **7**, 33 (1993).
[10]T. Oshio, Y. Sakai, and S. Ehara, J. Vac. Sci. Technol. B **12**, 2055 (2009).
[11]R. L. Smith, W. Lu, and G. S. Rohrer, Surf. Sci. **322**, 293 (1995).
[12]R. L. Smith, G. S. Rohrer, K. S. Lee, D. K. Seo, and M. H. Whangbo, Surf. Sci. **367**, 87 (1996).
[13]A. D. Costa, C. Mathieu, Y. Barbaux, H. Poelman, G. Dalmai-Vennik, and L. Fiermans, Surf. Sci. **370**, 339 (1997).
[14]M. V. Ganduglia-Pirovano and J. Sauer, Phys. Rev. B **70**, 45422 (2004).
[15]J. Goclon, R. Grybos, M. Witko, and J. Hafner, Phys. Rev. B **79**, 075439 (2009).
[16]B. Tepper, B. Richter, A. C. Dupuis, H. Kuhlenbeck, C. Hucho, and P. Schilbe, Surf. Sci. **496**, 64 (2002).

[17]G. Busca, G. Ramis, and V. Lorenzelli, J. Mol. Catal. **50**, 231 (1989).
[18]J. M. Sturm, D. Göbke, H. Kuhlenbeck, J. Döbler, U. Reinhardt, M. V. Ganduglia-Pirovano, J. Sauer, and H. J. Freund, Phys. Chem. Chem. Phys. **11**, 3290 (2009).
[19]D. Göbke, Y. Romanyshyn, S. Guimond, J. M. Sturm, H. Kuhlenbeck, J. Döbler, U. Reinhardt, M. V. Ganduglia-Pirovano, J. Sauer, and H. J. Freund, Angew. Chem., Int. Ed. **48**, 3695 (2009).
[20]X. Yin, H. Han, and A. Miyamoto, Phys. Chem. Chem. Phys. **2**, 4243 (2000).
[21]X. Yin, H. Han, A. Endou, M. Kubo, K. Teraishi, A. Chatterjee, and A. Miyamoto, J. Phys. Chem. B **103**, 1263 (1999).
[22]X. Yin, A. Fahmi, H. Han, A. Endou, S. S. C. Ammal, M. Kubo, K. Teraishi, and A. Miyamoto, J. Phys. Chem. B **103**, 3218 (1999).
[23]V. A. Ranea, J. L. Vicente, E. E. Mola, and R. U. Mananu, Surf. Sci. **442**, 498 (1999).
[24]K. Hermann, M. Witko, R. Druzinic, and R. Tokarz, Top. Catal. **11**, 67 (2000).
[25]G. Kresse and J. Furthmüller, Comp. Mat. Sci. **6**, 15 (1996).
[26]J. P. Perdew, K. Burke, and M. Ernzerhof, Phys. Rev. Lett. **77**, 3865 (1996).
[27]P. E. Blochl, Phys. Rev. B **50**, 17953 (1994).
[28]H. J. Monkhorst and J. D. Pack, Phys. Rev. B **13**, 5188 (1976).
[29]V. Brazdova, M. V. Ganduglia-Pirovano, and J. Sauer, Phys. Rev. B **69**, 165420 (2004).
[30]R. Enjalbert and J. Galy, Acta Crystallogr. Sect. C **42**, 1467 (1986).
[31]J. Goclon, R. Grybos, M. Witko, and J. Hafner, J. Phys. Condens. Matter **21**, 095008 (2009).
[32]G. Kresse, S. Surnev, M. G. Ramsey, and F. P. Netzer, Surf. Sci. **492**, 329 (2001).
[33]R. P. Blum, H. Niehus, C. Hucho, R. Fortrie, M. V. Ganduglia-Pirovano, J. Sauer, S. Shaikhutdinov, and H. J. Freund, Phys. Rev. Lett. **99**, 226103 (2007).
[34]S. E. Mason, C. R. Iceman, T. P. Trainor, and A. M. Chaka, Phys. Rev. B **81**, 125423 (2010).
[35]K. Reuter and M. Scheffler, Phys. Rev. B **65**, 035406 (2001).
[36]E. J. Granite, H. W. Pennline, and R. A. Hargis, Ind. Eng. Chem. Res. **39**, 1020 (2000).
[37]See [http://www.iecm-online.com] for technical documentation and current public version of the software IECM (2007).
[38]J. Rogal and K. Reuter, Ab Initio Atomistic Thermodynamics for Surfaces: A primer, Educational Notes, RTO-EN-AVT-142 (2007).
[39]X. G. Wang, A. Chaka, and M. Scheffler, Phys. Rev. Lett. **84**, 3650 (2000).
[40]C. S. Lo, K. S. Tanwar, A. M. Chaka, and T. P. Trainor, Phys. Rev. B **75**, 075425 (2007).
[41]Q. Sun, K. Reuter, and M. Scheffler, Phys. Rev. B **67**, 205424 (2003).
[42]*NIST-JANAF Thermochemical Tables*, 4th ed., edited by J. Chase (American Chemical Society, Washington, DC, 1998).
[43]Y. J. Kim, J. M. Lee, and S. D. Kim, Fuel **76**, 1067 (1997).
[44]K. Reuter and M. Scheffler, Phys. Rev. B **68**, 045407 (2003).
[45]*CRC Handbook of Chemistry and Physics*, 81st ed. (CRC Press, Boca Raton, FL, 2000).
[46]A. Eichler, F. Mittendorfer, and J. Hafner, Phys. Rev. B **62**, 4744 (2000).
[47]G. Henkelman, A. Arnaldsson, and H. Junsson, Comp. Mat. Sci. **36**, 354 (2006).
[48]J. Sauer and J. Döbler, Dalton Trans. **19**, 3116 (2004).
[49]G. Kresse, Phys. Rev. B **62**, 8295 (2000).
[50]F. Jachmann and C. Hucho, Solid State Commun. **135**, 440 (2005).
[51]R. J. Madix, J. Biener, M. Bumer, and A. Dinger, Faraday Discuss. **114**, 67 (1999).
[52]V. E. Henrich and P. A. Cox, *The Surface Science of Metal Oxides* (Cambridge University Press, Cambridge, 1996).